

# **Leveraging spaceborne lidar data for tropical ecosystem applications**

May, 2022

Savannah Cooley<sup>1,2\*</sup>, Naiara Pinto<sup>1</sup>

1 NASA Jet Propulsion Laboratory, California Institute of Technology, Pasadena, CA

2 Department of Ecology, Evolution, and Environmental Biology, Columbia University, New York, NY

## **Summary**

Here, we provide an overview of the use of light detection and ranging (lidar) for tropical ecosystem applications, with a particular focus on the Global Ecosystem Dynamics Investigation (GEDI). We summarize how data from GEDI measures vegetation vertical structure and give a step-by-step description of how to obtain spatially-subset GEDI Level 2A data from the NASA EarthData Search web portal. We then provide an example of how to characterize the structure of various vegetation classes in Ucayali, Peru. These vegetation classes include: (1) old-growth lowland forest, (2) young lowland vegetation regrowth ('Purma'), (3) secondary lowland forest, (4) mature oil palm plantations, and (5) cacao plantations (monocrop and agroforestry). We interpret the structural height metrics from GEDI among each of these vegetation classes, identifying edge effects as a possible influence on our results. To address this issue, we conducted a final analysis of the data with an area of 35m diameter footprint (25m of the original diameter area of the beam, and 10m as a conservative additional buffer) and excluded any observations that did not completely overlap with each land cover polygon. When we removed edge effects, no observations remained in the cacao data set and fewer observations remained in the forest stage data set. Nonetheless, the overall structural patterns shown in the relative heights of each forest stage remained very similar. We recommend that future projects utilizing spaceborne lidar for tropical ecosystems consider adopting the techniques and best practices we describe here, including refined noise filtering and explicit consideration of edge effects.

## **1. Lidar basics for tropical forests**

### **a. Characterizing tropical forest structure across spatial scales**

The ability to characterize tropical forest structure advances basic science and applications in land cover mapping, biodiversity recovery, sustainable supply chain initiatives and climate change mitigation, among others (Mattocha et al., 2012; Rogelj et al., 2018; Trabucco et al., 2008). Tropical forests are often considered the most structurally complex and yet least understood of forested ecosystems (Palace et al., 2016; Whitmore, 1982).

Variation in tropical forest structure can be observed across continental (Malhi et al., 2014), landscape (Chazdon et al., 2016) and even local scales (Norden et al., 2015). Tropical forest structure varies among these spatial scales in terms of differences in horizontal and vertical organization of the canopy. In addition to forest age (time since disturbance), a wide array of climate and environmental factors also play a role in determining vertical and horizontal canopy structure (Brown & Lugo, 1990; Shaw, 2004). At the local scale, light environments and forest community demographics can create complex dynamic feedbacks with forest structure (Stark et al., 2015). This variability in forest structure influences the extent to which tropical forests can

provide the biodiversity, livelihood, and carbon sequestration that land stewardship planning efforts depend on.

Most forest structure studies to-date focus on chronosequences and field experiments at the plot-scale (Chazdon et al., 2007; DeWalt et al., 2003; Guariguata & Ostertag, 2001; Peña-Claros, 2003) or airborne lidar measurements at the local scale (Drake et al., 2002; Drake et al., 2003; Clark et al., 2021; Feldpausch et al., 2005; Palace et al., 2016; Stark et al., 2015). At both of these scales, many potentially important landscape factors remain relatively constant. In contrast, there is much less known about the structure of forest canopies across landscape, regional and global scales (Clark et al., 2021; Feldpausch et al., 2005; Palace et al., 2016; Rödig et al., 2019).

### b. The use of Lidar to measure vegetation vertical structure

Lidar (light detection and ranging) offers an effective means to characterize forest structure across large spatial scales (Wulder et al., 2012). Spaceborne lidar uses laser light pulses to measure 3D structure, producing a single observable known as a "full-waveform". The emitted light is reflected by the land surface and clouds and then observed by a telescope in the spaceborne lidar system. Detectors convert the brightness of the reflected photons to an electronic voltage recorded as a function of time (based on the time difference between the firing of the laser and the detection of the backscattered signal). Finally, time is converted to a vertically resolved profile (i.e., distance) by multiplying time by the speed of light. The recorded voltage as a function of distance is the full-waveform.

In a small footprint airborne waveform lidar system, the waveform signal is typically decomposed into discrete x, y, and z points. These points are used in a similar manner as discrete return small-footprint data. The main advantages of waveform decomposition over the use of discrete return data are the increase in the number of echoes for each pulse (Persson et al., 2005) and knowledge of the algorithms used to extract the echoes (commercial discrete return systems use proprietary echo trigger mechanisms that are not known to the scientific community). For many years, however, mapping large areas with airborne waveform lidar remained challenging due to the logistics, costs, and data volumes involved. Utilizing spaceborne lidar as a sampling tool for large-area estimation can mitigate many of these challenges (Wulder et al., 2012).

Accurate three-dimensional models of the forest can be constructed from spaceborne lidar laser pulses by analyzing the time delay from pulse emission to return (i.e., the time of interaction with forest targets of the ground, branches, and leaves; Fig 1). The returned energy of each waveform can then be processed to determine elevation, canopy height, and relative height (RH) metrics. RH metrics define the percentage of the received laser waveform intensity that is less than a given height, where height is computed relative to the elevation of the lowest mode in the waveform. RH100 is the height of the highest return, which is considered to be the maximum canopy height. In practice, we usually use RH 95 due to issues distinguishing between signal and noise. Each RH percentile depends on the forest structure. For example, if a forest has a thick canopy or a tall understory, RH 50 and RH75 will be relatively high and closer to RH 100 compared to a forest with low or sparse understory and an upper canopy that doesn't have as much closure.

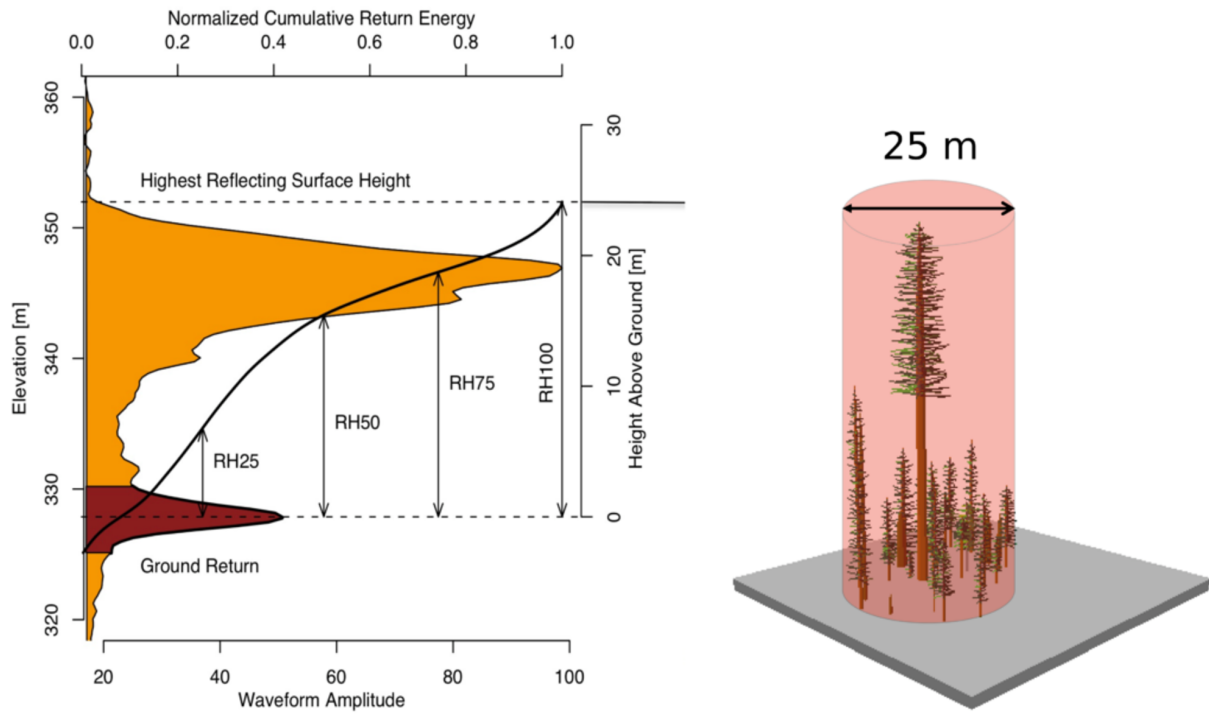


**Figure 1:** Conceptual diagram of a waveform (credit: NASA / GEDI mission). The returned energy of the waveform is processed to determine elevation, canopy height, and relative height (RH) metrics. RH metrics define the percentage of the received laser waveform intensity that is less than a given height, where height is computed relative to the elevation of the lowest mode in the waveform. The x axis represents the amount of energy in each return and the y axis shows the associated height (right axis) and elevation (left axis). The vertical lines show the RH metrics.

## 2. Characterizing tropical forest structure with NASA's GEDI mission

### a. Overview of the Global Ecosystem Dynamics Investigation (GEDI)

For the first time, forest structure can be assessed at landscape and global scales using new active remote sensing technologies, including NASA's recently launched Global Ecosystem Dynamics Investigation (GEDI), a light detection and ranging (lidar) instrument onboard the International Space Station (Dubayah et al., 2020). GEDI is optimized for characterizing forest structure. This is due to the non-polar orbit of the International Space Station (Fig 2), the high vertical accuracy of GEDI data (~50 cm) as well as the selection of the near-infrared portion of the electromagnetic spectrum for the GEDI laser pulses.

GEDI consists of 3 lasers, one of which is split into two beams ("coverage" beams), while the other two remain at full power ("power" beams). Each laser fires 242 times per second. A total of 4 laser beams are incident on the ground at any given time. These 4 beams produce 8 tracks of data, separated by about 600 m across the flight track direction within a ~4.2 km swath. Each GEDI beam footprint has a diameter of ~25 m. Footprint centers are separated by 60 m along track, or equivalently, 35 m from one edge to the next.

### b. GEDI Level 2A data description

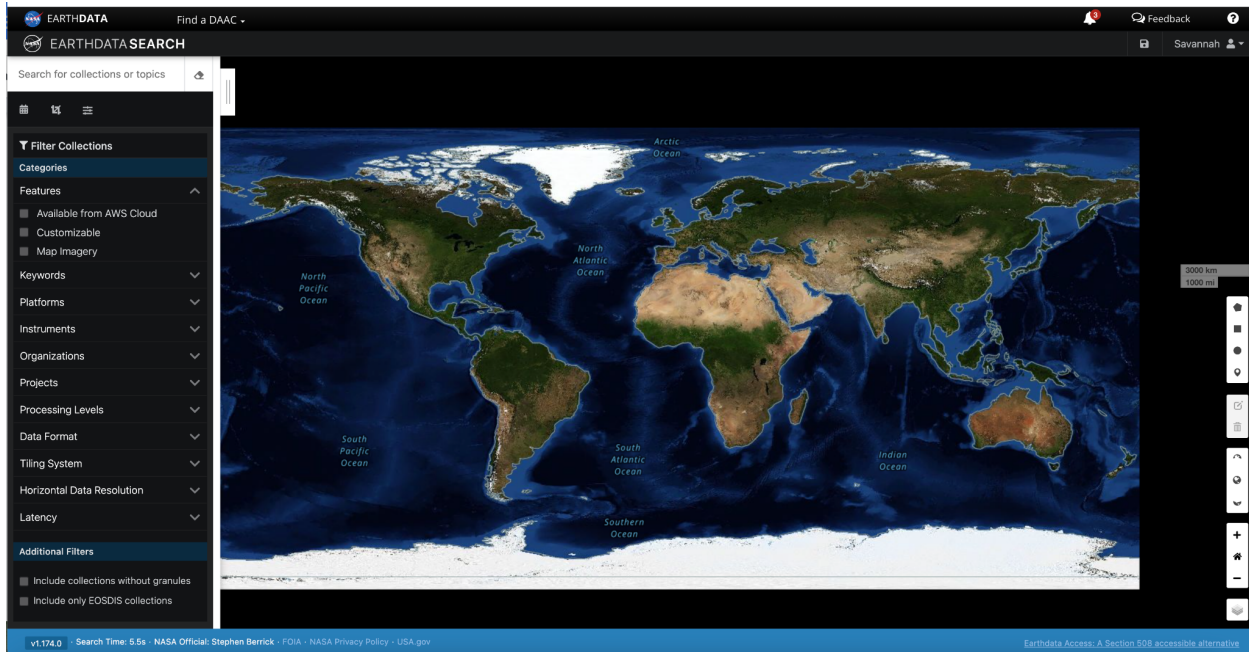
The purpose of the GEDI Level 2A Geolocated Elevation and Height Metrics product (GEDI02\_A) is to provide waveform interpretation and extracted products from each GEDI01\_B received waveform, including ground elevation, canopy top height, and relative height (RH) metrics. The methodology for generating the GEDI02\_A product datasets is adapted from the Land, Vegetation, and Ice Sensor (LVIS) algorithm.

The GEDI02\_A product is provided in HDF5 format and has a spatial resolution (average footprint) of 25 meters. The data product contains 156 layers for each of the eight beams, including ground elevation, canopy top height, relative return energy metrics (describing canopy vertical structure, as shown in Fig. 1), and many other interpreted products from the return waveforms. Additional information for the layers can be found in the [GEDI L2A Product Data Dictionary](#).

### c. How to search and spatially subset GEDI Level 2A data

This subsection provides a step-by-step description of how to search and spatially subset GEDI02\_A data.

- i. The first step to obtain GEDI02\_A data is to login to your EarthData Login Profile. If you do not have an existing account, you can create an account by registering [here](#).
- ii. Second, identify your area of interest with a geospatially enabled vector file that can be read by a geographic information system (e.g., geojson, shapefile or kml file).
- iii. Next, navigate to the EarthData Search web page.



- iv. Type the data product of interest (“GEDI02\_A”) and select the product from the list (full name: “GEDI L2A Elevation and Height Metrics Data Global Footprint Level V002”).

Granule ID	Start Date	End Date
GEDI02_A_2022075230117_O18456_01_T08568_02_003_02_V002.h5	2022-03-16 23:01:17	2022-03-17 00:34:10
GEDI02_A_2022075230117_O18456_02_T08568_02_003_02_V002.h5	2022-03-16 23:01:17	2022-03-17 00:34:10
GEDI02_A_2022075230117_O18456_03_T08568_02_003_02_V002.h5	2022-03-16 23:01:17	2022-03-17 00:34:10
GEDI02_A_2022075212824_O18455_01_T05721_02_003_02_V002.h5	2022-03-16 21:28:24	2022-03-16 23:01:17
GEDI02_A_2022075212824_O18455_02_T05721_02_003_02_V002.h5	2022-03-16 21:28:24	2022-03-16 23:01:17
GEDI02_A_2022075212824_O18455_03_T05721_02_003_02_V002.h5	2022-03-16 21:28:24	2022-03-16 23:01:17
GEDI02_A_2022075212824_O18455_04_T05721_02_003_02_V002.h5	2022-03-16 21:28:24	2022-03-16 23:01:17
GEDI02_A_2022075212824_O18455_05_T05721_02_003_02_V002.h5	2022-03-16 21:28:24	2022-03-16 23:01:17
GEDI02_A_2022075212824_O18455_06_T05721_02_003_02_V002.h5	2022-03-16 21:28:24	2022-03-16 23:01:17
GEDI02_A_2022075212824_O18455_07_T05721_02_003_02_V002.h5	2022-03-16 21:28:24	2022-03-16 23:01:17
GEDI02_A_2022075212824_O18455_08_T05721_02_003_02_V002.h5	2022-03-16 21:28:24	2022-03-16 23:01:17
GEDI02_A_2022075212824_O18455_09_T05721_02_003_02_V002.h5	2022-03-16 21:28:24	2022-03-16 23:01:17
GEDI02_A_2022075212824_O18455_10_T05721_02_003_02_V002.h5	2022-03-16 21:28:24	2022-03-16 23:01:17
GEDI02_A_2022075212824_O18455_11_T05721_02_003_02_V002.h5	2022-03-16 21:28:24	2022-03-16 23:01:17
GEDI02_A_2022075212824_O18455_12_T05721_02_003_02_V002.h5	2022-03-16 21:28:24	2022-03-16 23:01:17
GEDI02_A_2022075212824_O18455_13_T05721_02_003_02_V002.h5	2022-03-16 21:28:24	2022-03-16 23:01:17
GEDI02_A_2022075212824_O18455_14_T05721_02_003_02_V002.h5	2022-03-16 21:28:24	2022-03-16 23:01:17
GEDI02_A_2022075212824_O18455_15_T05721_02_003_02_V002.h5	2022-03-16 21:28:24	2022-03-16 23:01:17
GEDI02_A_2022075212824_O18455_16_T05721_02_003_02_V002.h5	2022-03-16 21:28:24	2022-03-16 23:01:17
GEDI02_A_2022075212824_O18455_17_T05721_02_003_02_V002.h5	2022-03-16 21:28:24	2022-03-16 23:01:17
GEDI02_A_2022075212824_O18455_18_T05721_02_003_02_V002.h5	2022-03-16 21:28:24	2022-03-16 23:01:17
GEDI02_A_2022075212824_O18455_19_T05721_02_003_02_V002.h5	2022-03-16 21:28:24	2022-03-16 23:01:17
GEDI02_A_2022075212824_O18455_20_T05721_02_003_02_V002.h5	2022-03-16 21:28:24	2022-03-16 23:01:17

- v. Input the geospatial vector file of your area of interest (click on the subset button, then “File” > “Browse Files”). Alternatively, you can draw the area of interest directly on the map (click on “Polygon” option). You can also

insert a temporal search to limit the number of resulting GEDI observations to a given time period (“Start” and “End”).

The screenshot shows the Earthdata Search interface for the GEDI02\_A dataset. On the left, there are filters for Spatial (Shape File), Granule ID(s), Temporal (Start and End dates), Data Access (Browse images or Online), and Orbit Number. A modal window titled "Search by Shape File" is overlaid, asking the user to upload a shapefile. The main search results show 20 matching granules, each with a thumbnail, start date, end date, and orbit number. The map on the right displays the global footprint of the GEDI mission, with many green lines representing individual orbits.

- Click the green button that says “Download All”. Notice that the search results include all GEDI tracks that overlap your area of interest. However, these resulting files include tracks of data that extend beyond your area of interest as well. In the next step, you can spatially subset the results to only download data within the area of interest rather than the entire orbit.

The screenshot shows the Earthdata Search interface for the GEDI02\_A dataset, specifically targeting Peru. The search results list 20 matching granules, each with a thumbnail, start date, end date, and orbit number. The map on the right shows the Peruvian coastline and interior, with a dense network of green lines representing GEDI orbits. The interface includes filters for Spatial (Shape File), Granule ID(s), Temporal (Start and End dates), Data Access (Browse images or Online), and Orbit Number.

- To spatially subset the download results within the area of interest, first select the “Customize” option under “Select a data access method” (step 1). Under “Configure data customization options” (step 2), enter your email address and check the boxes to enable the spatial subsetting and use the Shapefile from the original search. You can temporally subset the data at this stage.

EARTHDATA SEARCH

Untitled Project

447 Granules 1 Collection 438.1 GB

**GEDI L2A Elevation and Height Metrics Data Global Footprint Level V002**

447 Granules Est. Size 438.1 GB

Select a data access method for each collection in your project before downloading.

**Edit Options**

**Configure data customization options**

Edit the options below to configure the customization and output options for the selected data product.

Email Address  (Required)  
A valid email address is required.

Include Metadata and Processing History

Spatial Subsetting (Optional)

Click to enable

Use Shapefiles from Search  
Complex shapefiles may take longer to process. You will receive an email when your files are finished processing.

North

West

East

South

MONTH Mar Apr May Jun Jul

v1.174.0 · Search Time: 4.6s · NASA Official: Stephen Barrick · FOIA · NASA Privacy Policy · USA.gov

- viii. If you are working in the tropics, make sure to select power beam modes only (BEAM0101, BEAM0110, BEAM1000 and BEAM1011).

EARTHDATA SEARCH

Untitled Project

447 Granules 1 Collection 438.1 GB

**GEDI L2A Elevation and Height Metrics Data Global Footprint Level V002**

447 Granules Est. Size 438.1 GB

Select a data access method for each collection in your project before downloading.

**Edit Options**

Start Date

End Date

Band Subsetting (Optional)

Choose Bands

2160 of 4320 bands selected

GEDI02\_A

- BEAM0000
- BEAM0001
- BEAM0010
- BEAM0011
- BEAM0101
- BEAM0110
- BEAM1000
- BEAM1011

MONTH Mar Apr May Jun Jul

v1.174.0 · Search Time: 4.6s · NASA Official: Stephen Barrick · FOIA · NASA Privacy Policy · USA.gov

- ix. To complete your request, click “Done” and “Download Data.” You will receive an email from NASA/USGS LPDAAC confirming your order. When your order is complete, you will receive another email to download the data.

d. Spaceborne lidar limitations

i. Spatial coverage

GEDI is onboard the International Space Station (ISS) in the Japanese Experiment Module-Exposed Facility of the ISS (Fig 2B, 2C). Due to the orbit of the ISS, the spatial coverage of GEDI is limited to ~52 degrees north and south of the equator (Fig 2A).

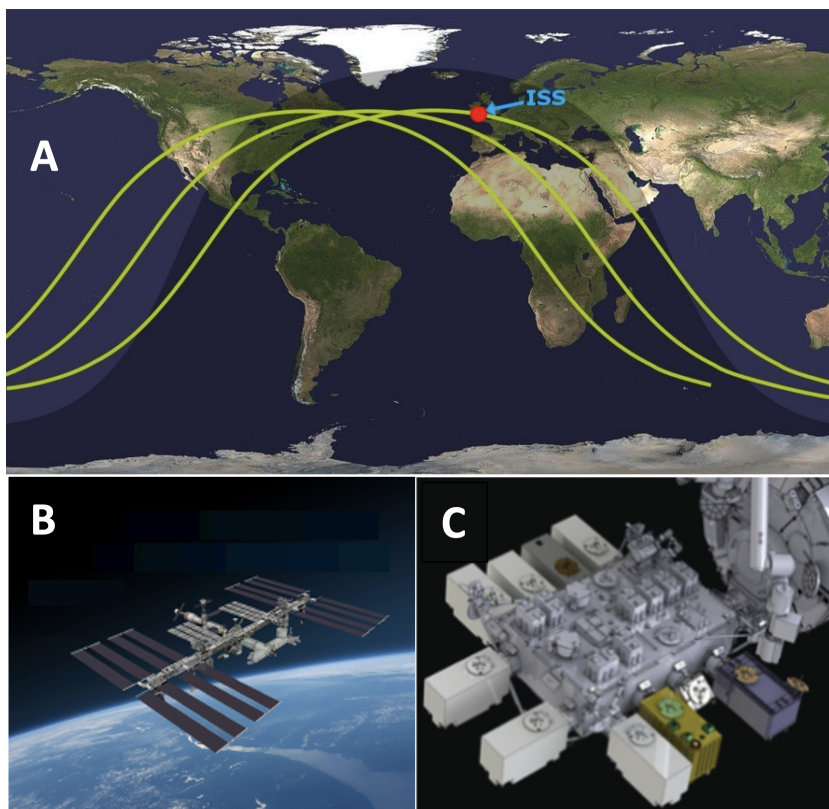


**Figure 2:** (A) Demonstration of the non-polar orbit of the International Space Station (ISS), which remains between ~52 degrees north and south of the equator (*image credit: Science ABC*). (B) Photo of the ISS (*image credit: NASA GEDI mission*). (C) Diagram of the placement of GEDI (highlighted in gold) on the Japanese Experiment Module-Exposed Facility of the ISS (*image credit: NASA GEDI mission*).

ii. Laser penetration in the tropics

For tropical forest applications, we recommend only using data from the full power beam modes.

Working with data from full power beams helps ensure that the data correspond to GEDI returns that penetrate the dense overstory canopy.

However, noise-removal filtering yields a highly unequal spatial distribution of GEDI data, with large data gaps over tropical forests (Potapov et al., 2021; Fig 3). GEDI data availability is low in tropical regions due to the impact of pervasive cloud cover on the number of high-quality GEDI samples available. The highest number of samples occurs in the northern part of the GEDI data range due to the orbit pattern of the ISS.

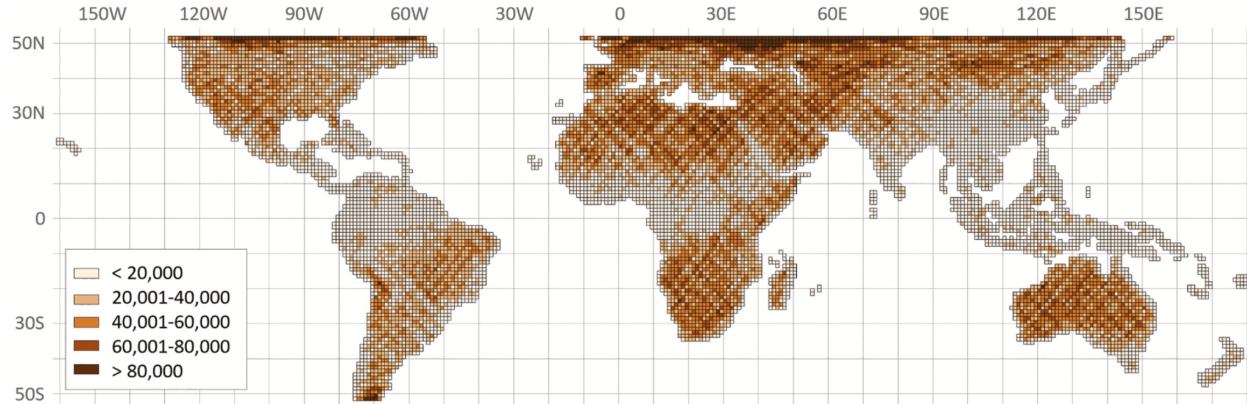


**Figure 3:** Number of GEDI samples available between April 18 and October 2, 2019 per  $1 \times 1^\circ$  grid tile used by Potapov et al. (2021) (credit: Potapov et al., 2021). Only high-quality samples were included (372 million samples total). The number of observations ranged from just a few samples to nearly 200,000 samples, with fewer high-quality observations available in the tropics due to high levels of noise.

### iii. Geolocation accuracy

Horizontal geolocation accuracy for the calibrated final products is  $\sim 10\text{m}$ . For this reason, we consider it a best practice to expand the range of GEDI observations to include an area of 35m diameter consisting of 25m from the original diameter area of the beam, and 10m as a conservative additional buffer to account for geolocation accuracy (Fig 4). In applications that aim to characterize distinct forest types and/or successional stages of regeneration, it is especially important to consider a 35m diameter area for each GEDI observation, where special attention must go toward ensuring homogeneity of the forest patch within the 35m diameter (i.e., eliminating observations where multiple forest types or edges occur in the larger conservative footprint area).

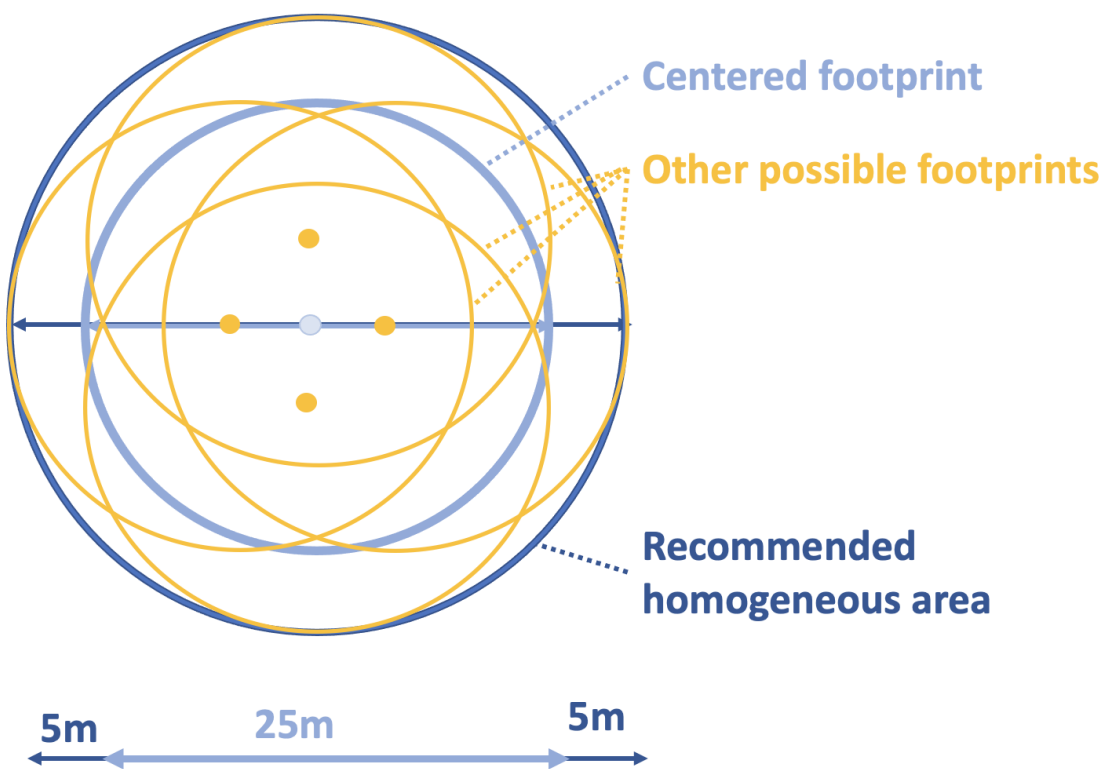


**Figure 4:** A best practice is to expand the range of GEDI observations to include an area of 35m diameter (25m of the original diameter area of the beam, and 10m as a conservative additional buffer to account for geolocation accuracy).

### 3. Application: Characteristic waveforms for old-growth and regenerating tropical lowland forest in Ucayali, Peru

Here, we plotted examples of relative height profiles for forest and agricultural regions in Ucayali, Peru. The vegetation classes included: (1) old-growth lowland forest, (2) young lowland vegetation regrowth ('Purma'), (3) secondary lowland forest, (4) mature oil palm plantations, and (5) cacao plantations (monocrop and agroforestry).

We selected all of the high quality (i.e. noise-filtered) GEDI observations available that spatially overlapped delineated vegetation class polygons from Cooley et al (in prep). The polygons were manually delineated using a combination of local expertise and high spatial resolution remote sensing images from MAXAR, Planet and Google Earth. See Cooley et al (2022) for more details about the methodology.

We applied the following noise filtering steps based on the methodology outlined by Potapov et al. (2020): (a) power beam mode only, (b) beam sensitivity  $\geq 0.9$  and (c)  $\leq 2\text{m}$  range of predicted ground elevations among the five algorithms after removing the algorithm that yielded the largest outlier elevation. For (c), we deviated from Potapov et al. (2020) and chose this approach to retain some observations that otherwise would have been removed if applying the  $\leq 2\text{m}$  range threshold to all six algorithms.

Overall, mature lowland forests exhibit the tallest canopy height (29.4m) relative to both of the other forest classes (secondary lowland forest is 20.82m and Young vegetation regrowth is 5.55m) as well as the agricultural classes (Cacao - monocrop is 6.0m, Cacao - agroforestry is 7.71m and Oil palm is 5.54m) (Table 1). The highest standard deviation in canopy height arises in the secondary forest class (9.15m) while the lowest standard deviation in canopy height occurs in the young vegetation regrowth class (3.55m).

In terms of vertical structure, secondary lowland forests exhibit a very similar vertical profile to mature lowland forests, with each relative height percentile increasing at similar rates (Figure 5). In contrast, young vegetation regrowth forest class exhibits a much more gradual increase in height across each RH percentile.

LandCover	Max	Min	Q25	Median	Q75	Mean	SD	Count
Cacao - agroforestry	23.48	0	4.23	5.68	9.63	7.71	5.4	47
Cacao - monocrop	26.61	2.32	3.4	4.15	6.5	6.07	4.74	97
Oil palm	33.97	8.01	9.09	10.3	12.48	11.28	3.28	1612
Mature lowland forest	55.98	2.05	25.51	29.65	33.71	29.40	6.89	2061
secondary lowland forest	44.48	1.87	14.94	21.35	27.3	20.82	9.15	281

Young vegetation regrowth 15.65 2.13 3.07 4.22 6.64 5.55 3.55 46

**Table 1.** Summary statistics of canopy height (RH95 in m) for each land cover class in this analysis: agricultural classes including oil palm plantations (all monocrop) and cacao plantations (both monocrop and agroforestry); and tropical lowland forest regeneration classes including mature forest, secondary/ and young vegetation.

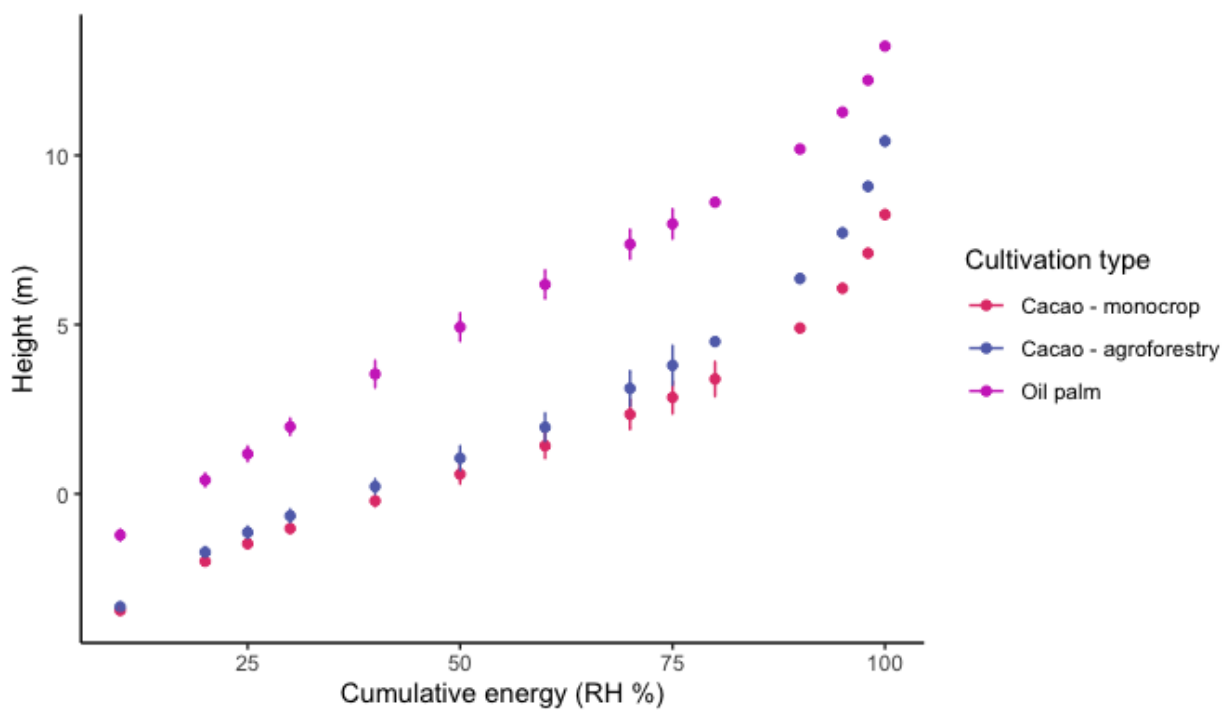
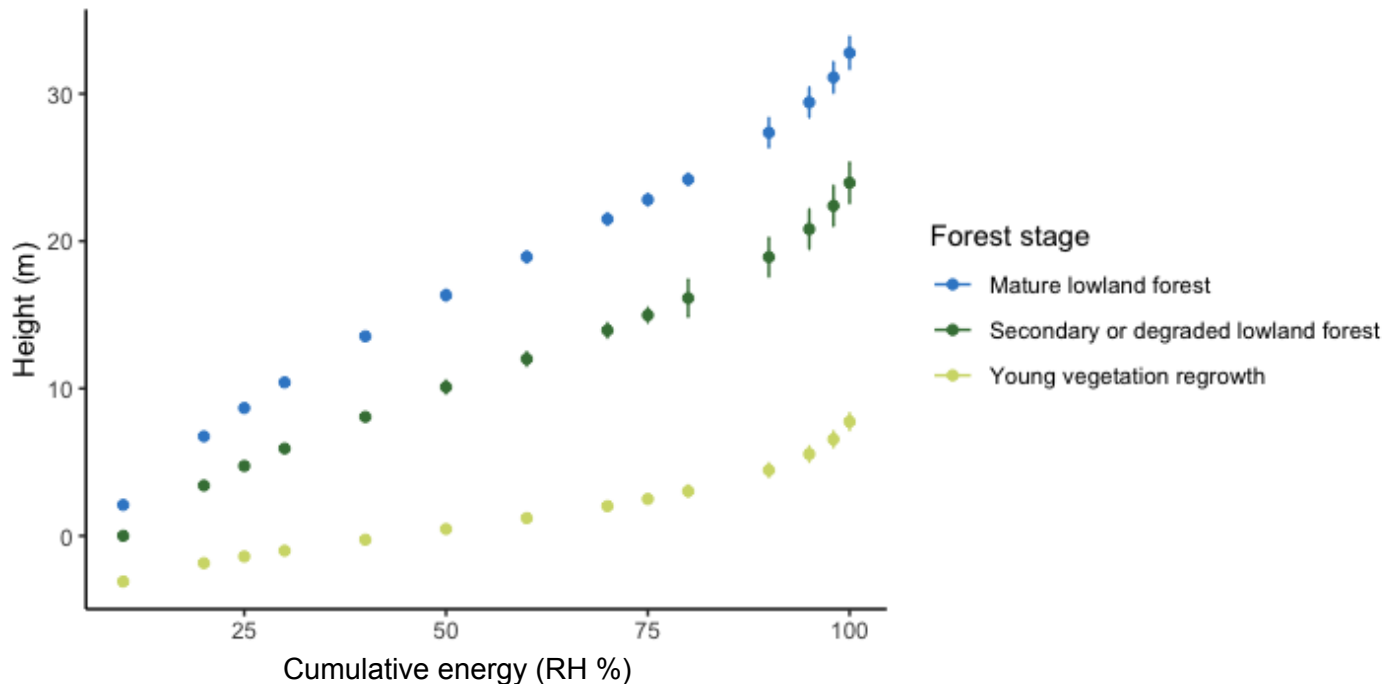


**Figure 5:** Characteristic waveform examples showing the mean and standard error of relative height metrics for (A) tropical lowland forest regeneration classes including mature forest, secondary/ and young vegetation ('urma'); and (B) agricultural classes including oil palm plantations (all monocrop) and cacao plantations (both monocrop and agroforestry).

The monocrop and agroforestry cacao cultivation types illustrate an even more remarkable structural similarity compared to the structural resemblance between mature lowland forests and secondary lowland forests. This similarity arises not only in terms of the rate of increase but also in terms of the magnitude of the relative height metrics. The vertical profile of the oil palm plantations also closely resembles the cacao plantations, though slightly decoupled (lower heights at each RH percentile after RH60 relative to the cacao plantations).

However, we suspected that one driver of our results is the influence of edge effects in the data (illustrated in Figure 4). For example, we observed that many of the GEDI observations that spatially coincide with the cacao plantations were not fully centered in the plantations but instead only partially overlapped with the plantations.

To address the edge effects, we included an area of 35m diameter footprint (25m of the original diameter area of the beam, and 10m as a conservative additional buffer) and excluded any observations that did not completely overlap with each land cover polygon. When we removed edge effects using a larger 35m diameter homogeneous area, no observations remained in the cacao data set and fewer observations remained in the forest stage data set. Nonetheless, the overall structural patterns shown in the relative heights of each forest stage remained very similar (Figure 6).

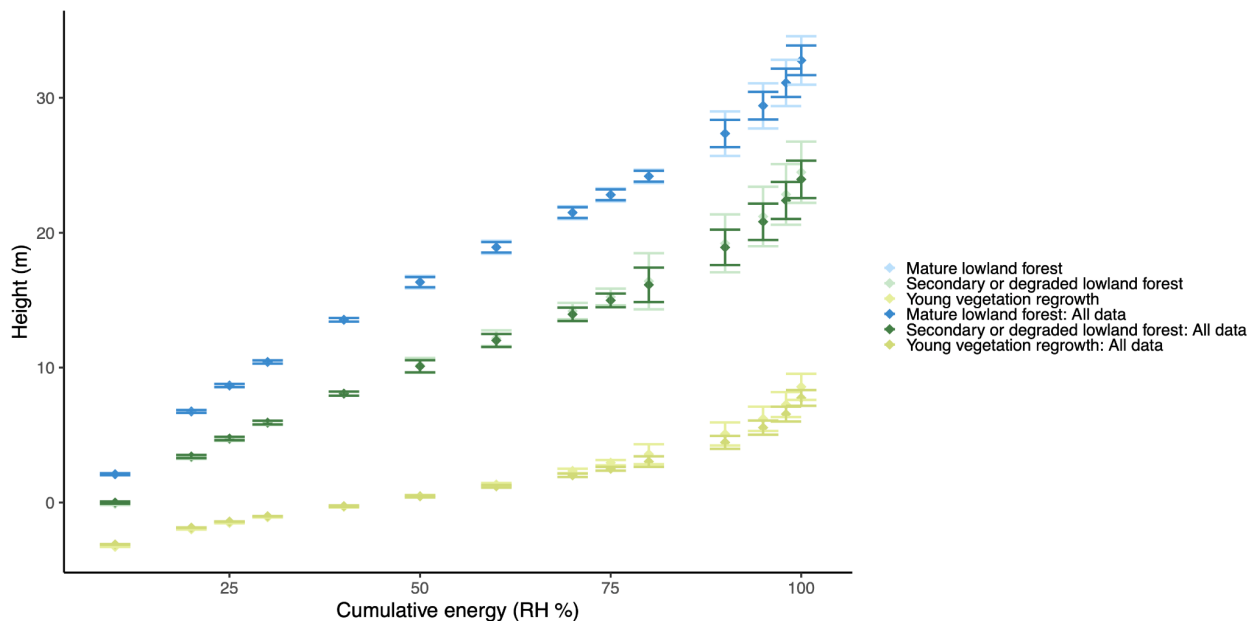


**Figure 6:** Difference in characteristic waveforms (mean and standard error of relative height metrics) when edge effects are removed (light colors) versus when all data are included (darker colors) for tropical lowland forest regeneration classes (mature forest, secondary forest and young vegetation).

#### **4. Conclusion**

Here, we provided an overview of the application of spaceborne lidar for characterizing tropical forest structure. This included a conceptual demonstration of full waveform lidar observations and an introduction to the Global Ecosystems Dynamics Investigation (GEDI) instrument onboard the International Space Station. We discuss the strengths and limitations of this instrument, including a description of data filtering steps that we recommend for tropical forest ecosystem applications. Using data from GEDI, we illustrated examples of relative height profiles for various forest and agriculture land cover classes in Ucayali, Peru.

## References

- Brown, S., & Lugo, A. E. (1990). Tropical secondary forests. *Journal of Tropical Ecology*, 6(1), 1–32. <https://doi.org/10.1017/S0266467400003989>
- Chazdon, R. L. (2017). Landscape Restoration, Natural Regeneration, and the Forests of the Future1. *Annals of the Missouri Botanical Garden*, 102(2), 251–257. <https://doi.org/10.3417/2016035>
- Chazdon, R. L., Letcher, S. G., van Breugel, M., Martínez-Ramos, M., Bongers, F., & Finegan, B. (2007). Rates of change in tree communities of secondary Neotropical forests following major disturbances. *Philosophical Transactions of the Royal Society B: Biological Sciences*, 362(1478), 273–289. <https://doi.org/10.1098/rstb.2006.1990>
- Clark, D. B., Oberbauer, S. F., Clark, D. A., Ryan, M. G., & Dubayah, R. O. (2021). Physical structure and biological composition of canopies in tropical secondary and old-growth forests. *PLOS ONE*, 16(8), e0256571. <https://doi.org/10.1371/journal.pone.0256571>
- DeWalt, S. J., Maliakal, S. K., & Denslow, J. S. (2003). Changes in vegetation structure and composition along a tropical forest chronosequence: Implications for wildlife. *Forest Ecology and Management*, 182(1), 139–151. [https://doi.org/10.1016/S0378-1127\(03\)00029-X](https://doi.org/10.1016/S0378-1127(03)00029-X)
- Drake, J. B., Dubayah, R. O., Knox, R. G., Clark, D. B., & Blair, J. B. (2002). Sensitivity of large-footprint lidar to canopy structure and biomass in a neotropical rainforest. *Remote Sensing of Environment*, 81(2), 378–392. [https://doi.org/10.1016/S0034-4257\(02\)00013-5](https://doi.org/10.1016/S0034-4257(02)00013-5)
- Drake, J. B., Knox, R. G., Dubayah, R. O., Clark, D. B., Condit, R., Blair, J. B., & Hofton, M. (2003). Above-ground biomass estimation in closed canopy Neotropical forests using lidar remote sensing: Factors affecting the generality of relationships. *Global Ecology and Biogeography*, 12(2), 147–159. <https://doi.org/10.1046/j.1466-822X.2003.00010.x>
- Dubayah, R., Blair, J. B., Goetz, S., Fatoyinbo, L., Hansen, M., Healey, S., Hofton, M., Hurt, G., Kellner, J., Luthcke, S., Armston, J., Tang, H., Duncanson, L., Hancock, S., Jantz, P., Marselis, S., Patterson, P. L., Qi, W., & Silva, C. (2020). The Global Ecosystem Dynamics Investigation: High-resolution laser ranging of the Earth's forests and topography. *Science of Remote Sensing*, 1, 100002. <https://doi.org/10.1016/j.srs.2020.100002>
- Feldpausch, T. R., Riha, S. J., Fernandes, E. C. M., & Wandelli, E. V. (2005). Development of Forest Structure and Leaf Area in Secondary Forests Regenerating on Abandoned Pastures in Central Amazônia. *Earth Interactions*, 9(6), 1–22. <https://doi.org/10.1175/EI140.1>
- Guariguata, M. R., & Ostertag, R. (2001). Neotropical secondary forest succession: Changes in structural and functional characteristics. *Forest Ecology and Management*, 148(1), 185–206. [https://doi.org/10.1016/S0378-1127\(00\)00535-1](https://doi.org/10.1016/S0378-1127(00)00535-1)
- Malhi, Y., Gardner, T., & Goldsmith, G. (2014). *Tropical Forests in the Anthropocene | Annual Review of Environment and Resources*. <https://www-annualreviews-org.ezproxy.cul.columbia.edu/doi/full/10.1146/annurev-environ-030713-155141>
- Matocha, J., Schroth, G., Hills, T., & Hole, D. (2012). Integrating Climate Change Adaptation and Mitigation Through Agroforestry and Ecosystem Conservation. In P. K. R. Nair & D. Garrity (Eds.), *Agroforestry—The Future of Global Land Use* (pp. 105–126). Springer Netherlands. [https://doi.org/10.1007/978-94-007-4676-3\\_9](https://doi.org/10.1007/978-94-007-4676-3_9)
- Norden, N., Angarita, H. A., Bongers, F., Martínez-Ramos, M., Cerda, I. G. la, Breugel, M. van, Lebrija-Trejos, E., Meave, J. A., Vandermeer, J., Williamson, G. B., Finegan, B., Mesquita, R., & Chazdon, R. L. (2015). Successional dynamics in Neotropical forests are as uncertain as they are predictable. *Proceedings of the National Academy of Sciences*, 112(26), 8013–8018. <https://doi.org/10.1073/pnas.1500403112>

- Palace, M., Sullivan, F. B., Ducey, M., & Herrick, C. (2016). Estimating Tropical Forest Structure Using a Terrestrial Lidar. *PLOS ONE*, 11(4), e0154115.  
<https://doi.org/10.1371/journal.pone.0154115>
- Peña-Claros, M. (2003). Changes in Forest Structure and Species Composition during Secondary Forest Succession in the Bolivian Amazon. *Biotropica*, 35(4), 450–461.  
<https://doi.org/10.1111/j.1744-7429.2003.tb00602.x>
- Potapov, P., Li, X., Hernandez-Serna, A., Tyukavina, A., Hansen, M. C., Kommareddy, A., Pickens, A., Turubanova, S., Tang, H., Silva, C. E., Armston, J., Dubayah, R., Blair, J. B., & Hofton, M. (2021). Mapping global forest canopy height through integration of GEDI and Landsat data. *Remote Sensing of Environment*, 253, 112165.  
<https://doi.org/10.1016/j.rse.2020.112165>
- Reitberger, J., Krzystek, P., & Stilla, U. (2008). Analysis of full waveform LIDAR data for the classification of deciduous and coniferous trees. *International Journal of Remote Sensing*, 29(5), 1407–1431. <https://doi.org/10.1080/01431160701736448>
- Rödig, E., Knapp, N., Fischer, R., Bohn, F. J., Dubayah, R., Tang, H., & Huth, A. (2019). From small-scale forest structure to Amazon-wide carbon estimates. *Nature Communications*, 10(1), 5088. <https://doi.org/10.1038/s41467-019-13063-y>
- Rogelj, J., Shindell, D., Jiang, K., Fifita, S., Forster, P., Ginzburg, V., Handa, C., Kheshgi, H., Kobayashi, S., Kriegler, E., Mundaca, L., Séférian, R., Vilarino, M. V., Calvin, K., de Oliveira de Portugal Pereira, J. C., Edelenbosch, O., Emmerling, J., Fuss, S., Gasser, T., ... Zickfeld, K. (2018). Mitigation Pathways Compatible with 1.5°C in the Context of Sustainable Development. *Global Warming of 1.5 °C*, 93–174.
- Shaw, D. (2004). Vertical Organization of Canopy Biota. In M. D. Lowman & H. B. Rinker (Eds.), *Forest Canopies* (pp. 73–102). Elsevier Academic Press.
- Stark, S. C., Enquist, B. J., Saleska, S. R., Leitold, V., Schietti, J., Longo, M., Alves, L. F., Camargo, P. B., & Oliveira, R. C. (2015). Linking canopy leaf area and light environments with tree size distributions to explain Amazon forest demography. *Ecology Letters*, 18(7), 636–645.  
<https://doi.org/10.1111/ele.12440>
- Trabucco, A., Zomer, R. J., Bossio, D. A., van Straaten, O., & Verchot, L. V. (2008). Climate change mitigation through afforestation/reforestation: A global analysis of hydrologic impacts with four case studies. *Agriculture, Ecosystems & Environment*, 126(1), 81–97.  
<https://doi.org/10.1016/j.agee.2008.01.015>
- Whitmore, T. C. (1982). On pattern and process in forests. *Special Publications Series of the British Ecological Society*.  
[https://scholar.google.com/scholar\\_lookup?title=On+pattern+and+process+in+forests&author=Whitmore%2C+T.C.&publication\\_year=1982](https://scholar.google.com/scholar_lookup?title=On+pattern+and+process+in+forests&author=Whitmore%2C+T.C.&publication_year=1982)
- Wulder, M. A., White, J. C., Nelson, R. F., Næsset, E., Ørka, H. O., Coops, N. C., Hilker, T., Bater, C. W., & Gobakken, T. (2012). Lidar sampling for large-area forest characterization: A review. *Remote Sensing of Environment*, 121, 196–209.  
<https://doi.org/10.1016/j.rse.2012.02.001>